Spin-mixing dynamics of a spinor Bose-Einstein condensate

H. Pu,[1] C. K. Law,[2] S. Raghavan,[3] J. H. Eberly,[3] and N. P. Bigelow[1]
[1]*Laboratory for Laser Energetics, and Department of Physics and Astronomy, University of Rochester, Rochester, New York 14627*
[2]*Department of Physics, The Chinese University of Hong Kong, Shatin, NT, Hong Kong, China*
[3]*Rochester Theory Center for Optical Science and Engineering and Department of Physics and Astronomy, University of Rochester, Rochester, New York 14627*
(Received 2 February 1999)

We study the spin-mixing dynamics of an $f=1$ spinor condensate. We show that the dynamics is sensitive to the relative phase and particle number distribution among the individual components of the condensate, and find that complex structures can develop in the density profiles during the time evolution. We investigate the different time scales of the spin-mixing process and their dependence on the total particle number. [S1050-2947(99)01308-6]

PACS number(s): 03.75.Fi, 05.30.Jp

I. INTRODUCTION

Experiments on dilute alkali-metal vapor condensates with internal degrees of freedom have opened up new areas in the study of Bose-Einstein condensation. Such a system was first realized in JILA where a magnetically confined Bose condensate composed of two hyperfine spin states of ^{87}Rb atoms was produced via sympathetic cooling [1] and, later, via a two-photon transition [2]. Interesting phenomena such as suppression of phase diffusion and interference effects have been studied both theoretically [3,4] and experimentally [5]. Recently, the MIT group have realized a condensate composed of all three hyperfine states of the $f=1$ ground-state multiplet of ^{23}Na atoms in a far-off-resonant optical dipole trap [6]. Besides the number of spin states involved, a major difference between the JILA condensate and the MIT condensate is that in the former, the bare energies of the two spin states are separated by about 7 GHz, hence the two spin components are not free to convert into each other without external couplings such as microwave pulses, while in the latter, the energy levels of all three spin states are degenerate in the absence of magnetic fields. The spin degree of freedom is completely released under this condition, and population can be transferred from one spin state to another under internal nonlinear interactions without the presence of external fields. The properties of such a three-component spinor condensate confined in a trap were studied by Ho [7], Ohmi and Machida [8], Goldstein and Meystre [9], and, more recently, by three of us [10]. A key feature of this system is that besides the usual two-body repulsive hard-core interactions, there also exist spin-exchange interactions that cause spin mixing within the condensate. In Ref. [10], we used a model to describe such interactions and we constructed a simple algebraic representation of the total Hamiltonian, from which we readily found a set of collective spin states as the ground-state of the spinor condensate.

In this paper, we extend the work presented in Ref. [10]. But instead of focusing on the ground state structure, here we investigate the more complete dynamics of a spinor condensate confined in a harmonic trap under the spin-exchange interactions. We show that the time evolution of a spinor condensate depends on the relative phase of the wave functions and the population distribution among different spin components, as well as on the total particle number. This study will help us gain insight into such properties as quantum phase diffusion, particle number fluctuations, spatial domain formation, etc.

This paper is organized as follows. In Sec. II we study the spin-mixing dynamics under the single-mode approximation (SMA) — all three spin states can be described by the same wave function whose spatial profile is time-independent. The SMA allows us to construct a set of angular momentum operators to describe the Hamiltonian of the condensate [10], with which we study the evolution of the condensate by assuming that the condensate is in a Fock state. These results will be presented in Sec. II A. In Sec. II B, we adopt the conventional view that a condensate is in a coherent state associated with a macroscopic wave function with both amplitude and phase. To this end, we treat the operators in Sec. II A as *c* numbers and derive three coupled differential equations to describe the condensate evolution and show how the evolution depends on the phase and particle number distributions in an individual spin state. We examine the limit of the validity of the SMA in Sec. III, where we derive a set of coupled nonlinear Schrödinger-like equations which we use to study the condensate dynamics numerically. We show that under certain conditions, the SMA becomes invalid and complex spatial structures develop in the spatial density profile of the condensate during the time evolution as a result of the mixing of various excitation modes. Finally, some concluding remarks are given in Sec. IV.

II. SPIN-MIXING DYNAMICS UNDER THE SMA

A. Angular momentum algebra for the spinor condensate

First, let us briefly review the algebraic method presented in Ref. [10]. We use the following general form for the two-body nonlinear interaction [7,8,11]:

$$U(\mathbf{r}_1,\mathbf{r}_2)=\delta(\mathbf{r}_1-\mathbf{r}_2)\sum_{F=0}^{2} g_F \sum_{M_F=-F}^{F} |F,M_F\rangle\langle F,M_F|. \tag{1}$$

Here $|F,M_F\rangle$ is the total hyperfine spin state formed by two

atoms each with spin $f=1$, and $g_F \equiv 4\pi\hbar^2 a_F/M$ with a_F being the s-wave scattering length in the F channel. For bosons, only even F states contribute to the above summation. The interaction (1) preserves angular momentum and rotation symmetry in hyperfine spin space.

By expanding the total spin state $|F,M_F\rangle$ in terms of basis vectors $|f=1,m_f=\alpha\rangle \otimes |f=1,m_f=\beta\rangle$ ($\alpha,\beta=-1,0,1$ denote the three spin states), we obtain the Hamiltonian in the form of the sum of a symmetric part and a nonsymmetric part $\mathcal{H}=\mathcal{H}_S+\mathcal{H}_A$, where

$$\mathcal{H}_S=\sum_\alpha \int d\mathbf{r}\hat{\Psi}_\alpha^\dagger(\hat{T}+V_T)\hat{\Psi}_\alpha+\frac{\lambda_s}{2}\sum_{\alpha,\beta}\int d\mathbf{r}\hat{\Psi}_\alpha^\dagger\hat{\Psi}_\beta^\dagger\hat{\Psi}_\alpha\hat{\Psi}_\beta \tag{2}$$

and

$$\begin{aligned}\mathcal{H}_A=\frac{\lambda_a}{2}\int d\mathbf{r}(&\hat{\Psi}_1^\dagger\hat{\Psi}_1^\dagger\hat{\Psi}_1\hat{\Psi}_1+\hat{\Psi}_{-1}^\dagger\hat{\Psi}_{-1}^\dagger\hat{\Psi}_{-1}\hat{\Psi}_{-1}\\&+2\hat{\Psi}_1^\dagger\hat{\Psi}_0^\dagger\hat{\Psi}_1\hat{\Psi}_0+2\hat{\Psi}_{-1}^\dagger\hat{\Psi}_0^\dagger\hat{\Psi}_{-1}\hat{\Psi}_0\\&-2\hat{\Psi}_1^\dagger\hat{\Psi}_{-1}^\dagger\hat{\Psi}_1\hat{\Psi}_{-1}+2\hat{\Psi}_0^\dagger\hat{\Psi}_0^\dagger\hat{\Psi}_1\hat{\Psi}_{-1}\\&+2\hat{\Psi}_1^\dagger\hat{\Psi}_{-1}^\dagger\hat{\Psi}_0\hat{\Psi}_0).\end{aligned} \tag{3}$$

Here $\hat{T}$ is the kinetic energy operator, V_T is the trapping potential, which is assumed to be the same for all three components [7], $\lambda_s \equiv (g_0+2g_2)/3$, and $\lambda_a \equiv (g_2-g_0)/3$. The symmetric part $\mathcal{H}_S$ remains unchanged for any interchange of the spin-component indices.

Next, we assume that $|\lambda_s| \gg |\lambda_a|$ (recent estimates have indicated that both sodium and rubidium atoms indeed satisfy this assumption [7]) such that $\mathcal{H}_S$ dominates over $\mathcal{H}_A$. Hence, the wave functions for each spin component $\phi_\kappa(\mathbf{r})$ ($\kappa=0,\pm1$) are approximated by the same wave function $\phi(\mathbf{r})$ defined as the ground-state solution of the Gross-Pitaevskii equation resulting from $\mathcal{H}_S$ (the validity of this single-mode approximation will be discussed later):

$$(\hat{T}+V_T+\lambda_s N|\phi|^2)\phi=\mu\phi, \tag{4}$$

where N is the total particle number in the condensate and μ is the chemical potential. Now we can approximate the field operators in the zero-temperature limit by

$$\hat{\Psi}_\kappa \approx \hat{a}_\kappa \phi(\mathbf{r}), \quad \kappa=0,\pm1. \tag{5}$$

Here $\hat{a}_\kappa$ is the annihilation operator which obeys the usual boson commutation relations. Using Eqs. (4) and (5), the leading parts of $\mathcal{H}_S$ and $\mathcal{H}_A$, denoted by H_s and H_a, respectively, have the following expressions:

$$H_s=\mu\hat{N}-\lambda_s'\hat{N}(\hat{N}-1), \tag{6}$$

$$\begin{aligned}H_a=\lambda_a'(&\hat{a}_1^\dagger\hat{a}_1^\dagger\hat{a}_1\hat{a}_1+\hat{a}_{-1}^\dagger\hat{a}_{-1}^\dagger\hat{a}_{-1}\hat{a}_{-1}+2\hat{a}_1^\dagger\hat{a}_0^\dagger\hat{a}_1\hat{a}_0\\&+2\hat{a}_{-1}^\dagger\hat{a}_0^\dagger\hat{a}_{-1}\hat{a}_0-2\hat{a}_1^\dagger\hat{a}_{-1}^\dagger\hat{a}_1\hat{a}_{-1}+2\hat{a}_0^\dagger\hat{a}_0^\dagger\hat{a}_1\hat{a}_{-1}\\&+2\hat{a}_1^\dagger\hat{a}_{-1}^\dagger\hat{a}_0\hat{a}_0).\end{aligned} \tag{7}$$

Here $\lambda_i' \equiv (\lambda_i/2)\int d\mathbf{r}|\phi(\vec{x})|^4$ ($i=s,a$).

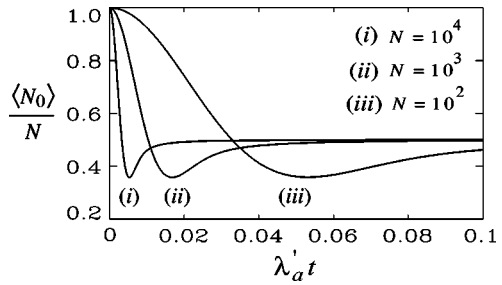

FIG. 1. Population of the spin-0 component as a function of time. The corresponding populations in the other two components are $\langle n_1\rangle=\langle n_{-1}\rangle=(N-\langle n_0\rangle)/2$. The initial state is $|\psi(t=0)\rangle=|0,N,0\rangle$.

Since the Hamiltonian conserves the total number of particles, and H_s is a function of $\hat{N}$ only, H_s is a constant operator. Hence, we need only to focus on the nonsymmetric part H_a. Following Refs. [10,12,13], we construct a set of angular momentum operators:

$$\begin{aligned}\hat{L}_- &\equiv \sqrt{2}(\hat{a}_1^\dagger\hat{a}_0+\hat{a}_0^\dagger\hat{a}_{-1}),\\ \hat{L}_+ &\equiv \sqrt{2}(\hat{a}_0^\dagger\hat{a}_1+\hat{a}_{-1}^\dagger\hat{a}_0),\\ \hat{L}_z &\equiv (\hat{a}_{-1}^\dagger\hat{a}_{-1}-\hat{a}_1^\dagger\hat{a}_1).\end{aligned} \tag{8}$$

Using the above operators, H_a takes a very simple form,

$$H_a=\lambda_a'(\hat{L}^2-2\hat{N}). \tag{9}$$

One can easily see that all three operators defined in Eq. (8) are constants of motion since they commute with both H_s and H_a. The energy spectrum of the total Hamiltonian $H=H_s+H_a$ is $E_T^{(l)}=E_s+E_a^{(l)}$, where

$$\begin{aligned}E_s &= \mu N-\lambda_s' N(N-1),\\ E_a^{(l)} &= \lambda_a'[l(l+1)-2N],\end{aligned}$$

where $l=0,2,4,\ldots,N$ if N is even, and $l=1,3,5,\ldots,N$ if N is odd. For fixed N, the lowest energy is

$$\begin{aligned}E_{\min}=E_T^{(0)}=E_s-2\lambda_a' N \ \text{ for } \ \lambda_a'>0,\\ E_{\min}=E_T^{(N)}=E_s+\lambda_a' N(N-1) \ \text{ for } \ \lambda_a'<0.\end{aligned}$$

Now let us assume that initially the condensate is in a Fock state $|N_{-1},N_0,N_1\rangle$ defined by the number operators $\hat{N}_j \equiv \hat{a}_j^\dagger\hat{a}_j$ for the three spin components (i.e., $\hat{N}_j|N_{-1},N_0,N_1\rangle=N_j|N_{-1},N_0,N_1\rangle$) and the total particle number $N=N_{-1}+N_0+N_1$. The time evolution of the condensate is governed by H_a in Eq. (9) and can be readily solved using the Fock state basis. Figures 1 –3 show the particle number in each spin component as functions of time given a certain initial state.

Figure 1 illustrates the spin mixing of an initially spin-polarized condensate with all the atoms in the spin-0 component at $t=0$, i.e., $|\psi(t=0)\rangle=|0,N,0\rangle$. The particle number distribution quickly collapses to a ''steady state'' with $\langle N_1\rangle_{ss}=\langle N_{-1}\rangle_{ss}=\langle N_0\rangle_{ss}/2=N/4$ [14], and the collapse time

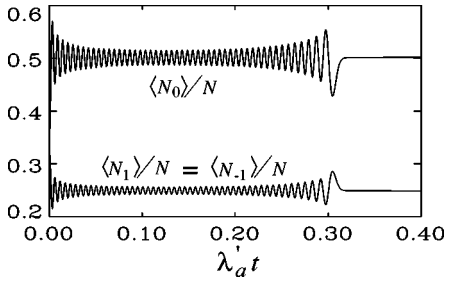

FIG. 2. Population of each spin component as a function of time. The initial state is $|\psi(t=0)\rangle=|N/3,N/3,N/3\rangle$. Here, $N=300$.

t_c is approximately given by $\lambda_a' t_c \approx 1/(2\sqrt{N})$. In the Thomas-Fermi limit, $\lambda_a' \sim N^{-3/5}$ in three dimensions (3D) and $\lambda_a' \sim N^{-1/3}$ in 1D, therefore, $t_c \sim N^{1/10}$ in 3D and $t_c \sim N^{-1/6}$ in 1D.

Figure 2 shows the time evolution of a condensate whose spin components are initially equally populated, i.e., $|\psi(t=0)\rangle=|N/3,N/3,N/3\rangle$. In this case, the particle number in each spin component executes oscillations before it settles to the steady-state value which is the same as in the previous case. The oscillation frequency ν is about $1.7\times\lambda_a' N$. In the Thomas-Fermi limit, $\nu \sim N^{2/5}$ in 3D and $\nu \sim N^{2/3}$ in 1D.

Figure 3 shows another example where initially the spin-0 and the spin-1 components are equally populated, while the spin-(-1) component is not populated, i.e., $|\psi(t=0)\rangle=|0,N/2,N/2\rangle$. In this case, the steady-state values for population in each component are $\langle N_{-1}\rangle_{ss}=N/12$, $\langle N_0\rangle_{ss}=N/3$, and $\langle N_1\rangle_{ss}=7N/12$. The system approaches the steady-state like a damped oscillator: The particle number in each component oscillates around its steady state value sinusoidally with the oscillation amplitude modulated by a Gaussian damping function. A good analytical functional fit to the data is

$$\langle N_i(t)\rangle - \langle N_i\rangle_{ss} \sim \cos(2\pi f t) e(-t^2/t_d^2),$$

where $f=0.55\lambda_a' N$ and $t_d=0.89/(\lambda_a'\sqrt{N})$. In the Thomas-Fermi limit, $f\sim N^{2/5}$ in 3D and $f\sim N^{2/3}$ in 1D; $t_d\sim N^{1/10}$ in 3D and $t_d\sim N^{-1/6}$ in 1D. Note that t_d has the same N dependence as t_c in Fig. 1, and f has the same N dependence as ν in Fig. 2. This is not surprising since the only difference between these three examples is the initial population distributions.

B. Condensate in coherent state: Semiclassical treatment

In the preceding subsection, we have assumed that the system can be represented by a Fock state $|N_1,N_0,N_{-1}\rangle$.

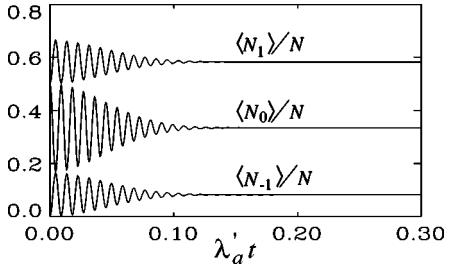

FIG. 3. Population of each spin component as a function of time. The initial state is $|\psi(t=0)\rangle=|0,N/2,N/2\rangle$, $N=200$.

However, it is customary to consider the condensate to be in a *coherent state*, associated with a macroscopic wave function with both magnitude and *phase*, the presence of which is due to the spontaneous breaking of gauge symmetry [15]. This is the view we will adopt here, to assume the condensate to be in such a coherent state with a definite phase in each spin component:

$$|\Phi\rangle=|a_{-1},a_0,a_1\rangle=|\sqrt{N_{-1}}e^{i\theta_{-1}},\sqrt{N_0}e^{i\theta_0},\sqrt{N_1}e^{i\theta_1}\rangle. \tag{10}$$

As the coherent state $|v\rangle$ is analogous to a classical field of complex amplitude v, it is customary to replace the operators $\hat{a}_i,\hat{a}_i^\dagger$ by c numbers a_i and a_i^*, respectively. The semiclassical equations of motion can be derived from Hamiltonian H_a as

$$\begin{aligned} i\dot{a}_{-1} &= 2\lambda_a'(L_z a_{-1}+L_- a_0/\sqrt{2}),\\ i\dot{a}_0 &= \sqrt{2}\lambda_a'(L_- a_1+L_+ a_{-1}),\\ i\dot{a}_1 &= 2\lambda_a'(-L_z a_1+L_+ a_0/\sqrt{2}), \end{aligned} \tag{11}$$

where the quantities $L_\pm, L_z$ are c number counterparts of the operators $\hat{L}_\pm$ and $\hat{L}_z$, respectively, and are therefore constants of motion determined by the initial values of a_i's. In deriving Eqs. (11), we have neglected the contribution from H_s which will give each of the three equations in Eq. (11) a constant energy shift $E_s a_i$ that can be trivially eliminated by changing a_i to $a_i e^{-iE_s t}$.

The eigenfrequencies of the system of Eqs. (11) are 0, $\pm\Omega=\pm 2|\lambda_a'|L$ with corresponding eigenvectors

$$|\varphi_0\rangle=\frac{1}{\sqrt{2L}}|-L_-,\sqrt{2}L_z,L_+\rangle, \tag{12a}$$

$$|\varphi_\pm\rangle=\frac{|L_+|}{|L_+|^2+\mathcal{A}_\pm^2}|\mathcal{A}_\pm^2/L_+,\sqrt{2}\mathcal{A}_\pm,L_+\rangle, \tag{12b}$$

where $L\equiv\sqrt{L_z^2+L_+L_-}$ and $\mathcal{A}_\pm\equiv L_z\pm L$.

Interestingly, eigenstate $|\varphi_0\rangle$ is orthogonal to the initial state (10), i.e., $\langle\varphi_0|\Phi\rangle=0$. The population in spin i at time t will be $P_i=|\langle i|\Phi(t)\rangle|^2/N$, with $|\Phi(t)\rangle$ given by

$$|\Phi(t)\rangle=\langle\varphi_+|\Phi\rangle|\varphi_+\rangle e^{i\Omega t}+\langle\varphi_-|\Phi\rangle|\varphi_-\rangle e^{-i\Omega t}.$$

Particularly, for states with $L_z=0$, i.e., $N_{-1}=N_1$, we have

$$\begin{aligned} P_0(\theta,t) &= 1/2-(1/2-n_0)\cos(2\Omega t)\\ &\quad -\sqrt{n_0(1-n_0)}\sin(\theta/2)\sin(2\Omega t),\\ P_1(\theta,t) &= P_{-1}(\theta,t)=[1-P_0(\theta,t)]/2, \end{aligned} \tag{13}$$

where $n_0=N_0/N$ is the initial population in spin-0, $\theta=2\theta_0-\theta_1-\theta_{-1}$ is the initial relative phase, and

$$\Omega=4|\lambda_a' N\sqrt{n_0(1-n_0)}\cos(\theta/2)|. \tag{14}$$

Hence we find that the population in each spin state oscillates with frequency 2Ω, the value of which depends on the

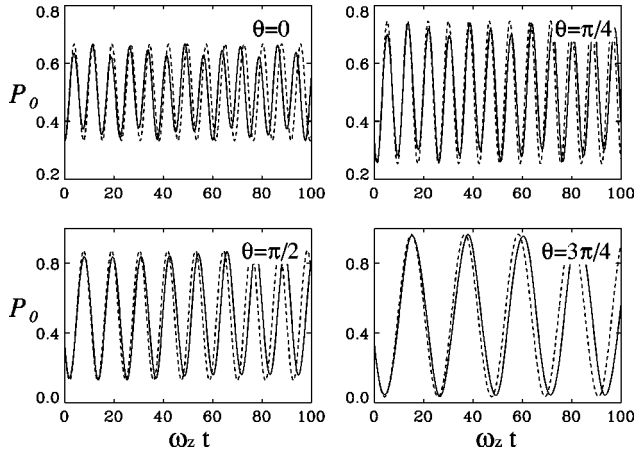

FIG. 4. Population of spin-0 component as a function of time. Initially, $n_1=n_0=n_{-1}$. Dashed lines: the SMA results according to Eq. (13); solid lines: numerical results of Sec. III. The parameters we used in the calculation are $\omega_z=2\pi\times 40$Hz, $\eta=1$, $a_0=46a_B$, $a_2=52a_B$ (a_B is the Bohr radius), $N=4000$.

initial phase and population of the condensate. For $L_z\neq 0$, the oscillation frequency Eq. (14) will be modified as

$$\Omega=2|\lambda_a'|N \times\sqrt{(n_{-1}-n_1)^2+2n_0(n_{-1}+n_1)+4n_0\sqrt{n_1n_{-1}}\cos\theta}. \tag{15}$$

Figure 4 illustrates $P_0(\theta,t)$ for several different values of θ and for the initial state that all three spin states are equally populated. Experimental observation of this population oscillation may help us determine the phase of the condensate.

Instead of assuming a definite phase, it will also be instructive to study the case that θ is not well determined. For example, let us assume that θ is uniformly distributed over the range $(0,2\pi]$. Integrating Eqs. (13) over θ gives

$$P_0(t)=\tfrac{1}{2}-(\tfrac{1}{2}-n_0)J_0\left(\frac{8\sqrt{2}}{3}|\lambda_a'|Nt\right), \tag{16}$$

where $J_0(x)$ is the zeroth-order ordinary Bessel function. An example is represented by the dashed lines in Fig. 5. In this

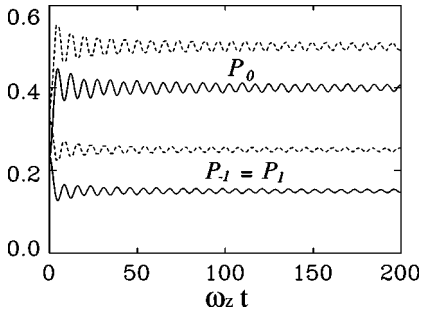

FIG. 5. Population of each spin component as a function of time, averaged over initial relative phase θ which is uniformly distributed over $(0,2\pi]$. Initially, $n_1=n_0=n_{-1}$. Dashed lines: the SMA results according to Eq. (16); solid lines: numerical results of Sec. III (shifted down by 0.1 for clarity). Same parameters as in Fig. 4.

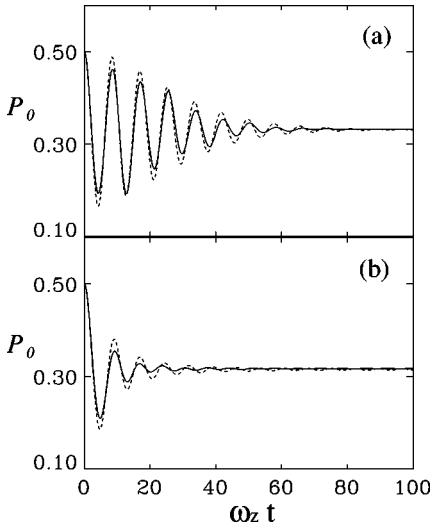

FIG. 6. Population of spin-0 component as a function of time, averaged over initial particle number distribution. Initially, n_1 and n_0 has a Gaussian distribution centered at $\frac{1}{2}$ with a width of $\Delta n_0=0.1$ for (a) and $\Delta n_0=0.4$ for (b); $n_{-1}=0$. Same parameters as in Fig. 4. Dashed lines are the SMA results of Sec. II and solid lines are numerical results of Sec. III.

case, the population distribution reaches a steady-state with $P_0(\infty)=1/2$ and $P_{-1}(\infty)=P_1(\infty)=1/4$. These values agree with the steady state values obtained using the Fock-state representation (see Fig. 1).

Next, we study a case that the initial population in each spin state is not well determined. Assume that the initial state is given by $|\Phi(0)\rangle=|0,\sqrt{N_0}e^{i\theta_0},\sqrt{N-N_0}e^{i\theta_1}\rangle$, where the population in spin-0, $n_0=N_0/N$, has a Gaussian distribution centered at $\frac{1}{2}$ with a width Δn_0: $p(n_0)=\mathcal{N}\exp[-(n_0-1/2)^2/(\Delta n_0)^2]$, where $\mathcal{N}$ is the normalization factor. After some algebra, we find that for a certain value of n_0, the population in spin-0 at time t is given by

$$P_0(n_0,t)=\frac{1-n_0}{2-n_0}[1+(1-n_0)\cos(2\Omega t)], \tag{17}$$

where $\Omega=2\lambda_a'N\sqrt{1-n_0^2}$ and the corresponding populations in the other two states are $P_{-1}(n_0,t)=[n_0-P_0(n_0,t)]/2$ and $P_1(n_0,t)=1-[n_0+P_0(n_0,t)]/2$. Taking the distribution $p(n_0)$ into account, we have $P_0(t)=\int_0^1 P_0(n_0,t)p(n_0)dn_0$, which is plotted in Fig. 6. We can see that the population reaches a steady state with $(P_{-1}(\infty),P_0(\infty),P_1(\infty))=(1/12,1/3,7/12)$ like a damped oscillator with oscillation frequency $f=0.55\lambda_a'N$. The damping time depends on the width Δn_0: the larger Δn_0 is, the faster it reaches equilibrium. Furthermore, for small Δn_0, the damping envelope is approximately a Gaussian, while for large Δn_0, it is closer to an exponential. For fixed Δn_0, the damping time is inversely proportional to $\lambda_a'N$. It is interesting that both the steady-state population and the oscillation frequency are the same as those presented in Fig. 3, where we have a Fock state $|0,N/2,N/2\rangle$ at $t=0$.

III. NUMERICAL METHOD BEYOND THE SMA

In Sec. II, we have assumed that during the time evolution, the wave functions for all spin components retain the

same spatial profile as defined in Eq. (4). Therefore, we could trace out the spatial dependence of the wave functions and focus on the change of the population in each spin component as a function of time. Now we study the spin-mixing dynamics of the spinor condensate by directly integrating the coupled nonlinear Schrödinger-like partial differential equations which include the time variation of the spatial wave functions. This allows us to study the complex structures developed in the density profiles of the condensate and also to examine the validity of the SMA.

A. Physical model

Denoting ψ_i as the wave function for spin-i, the equations of motion of ψ_i may be derived from Hamiltonians (2) and (3):

$$\begin{aligned} i\hbar\dot{\psi}_{-1} &= \mathcal{L}\psi_{-1}+\lambda_a N(\psi_0^2\psi_1^*+|\psi_{-1}|^2\psi_{-1}+|\psi_0|^2\psi_{-1} \\ &\quad -|\psi_1|^2\psi_{-1}), \\ i\hbar\dot{\psi}_0 &= \mathcal{L}\psi_0+\lambda_a N(2\psi_1\psi_{-1}\psi_0^*+|\psi_{-1}|^2\psi_0+|\psi_1|^2\psi_0), \\ i\hbar\dot{\psi}_1 &= \mathcal{L}\psi_1+\lambda_a N(\psi_0^2\psi_{-1}^*+|\psi_1|^2\psi_1+|\psi_0|^2\psi_1-|\psi_{-1}|^2\psi_1), \end{aligned} \tag{18}$$

where $\mathcal{L}=\hat{T}+V_T+\lambda_s N(|\psi_{-1}|^2+|\psi_0|^2+|\psi_1|^2)$ and ψ_i's are normalized such that $\int(|\psi_{-1}|^2+|\psi_0|^2+|\psi_1|^2)d\mathbf{r}=1$. We now assume that the trapping potential is a cigar-shaped harmonic potential with tight confinement in the transverse direction (this is indeed the case for the MIT experiment [6]), i.e.,

$$V_T=\frac{1}{2}m\omega_\perp^2(x^2+y^2)+\frac{1}{2}m\omega_z^2z^2 \quad \text{with} \quad \omega_\perp \gg \omega_z .$$

We approximate the transverse wave function of the condensate as the ground state of a two-dimensional harmonic oscillator (with transverse potential). Hence the wave function associated with the spin-i state may be written as [9]

$$\psi_i(x,y,z,t)=\phi_\perp(x,y)\,\phi_i(z,t)e^{-i\omega_\perp t}, \tag{19}$$

where $\phi_\perp(x,y)$ satisfies

$$\left[-\frac{\hbar^2}{2m}\nabla_\perp^2+\frac{1}{2}m\omega_\perp^2(x^2+y^2)\right]\phi_\perp(x,y)=\hbar\omega_\perp\phi_\perp(x,y).$$

Inserting Eqs. (19) into (18), we obtain the equations of motion for the longitudinal wave functions $\phi_i(z,t)$. In dimensionless form, these equations have the following expressions:

$$\begin{aligned} i\dot{\phi}_{-1} &= \mathcal{L}_z\phi_{-1}+\lambda_a N\eta(\phi_0^2\phi_1^*+|\phi_{-1}|^2\phi_{-1}+|\phi_0|^2\phi_{-1} \\ &\quad -|\phi_1|^2\phi_{-1}), \\ i\dot{\phi}_0 &= \mathcal{L}_z\phi_0+\lambda_a N\eta(2\phi_1\phi_{-1}\phi_0^*+|\phi_{-1}|^2\phi_0+|\phi_1|^2\phi_0), \\ i\dot{\phi}_1 &= \mathcal{L}_z\phi_1+\lambda_a N\eta(\phi_0^2\phi_{-1}^*+|\phi_1|^2\phi_1+|\phi_0|^2\phi_1 \\ &\quad -|\phi_{-1}|^2\phi_1), \end{aligned} \tag{20}$$

where $\mathcal{L}_z=-d^2/dz^2+z^2/4+\lambda_s N\eta(|\phi_{-1}|^2+|\phi_0|^2+|\phi_1|^2)$, and in dimensionless form,

$$\eta=\frac{\int dxdy|\phi_\perp(x,y)|^4}{\int dxdy|\phi_\perp(x,y)|^2}=\frac{1}{4\pi}\frac{\omega_\perp}{\omega_z}.$$

In the above equations, the units for length, energy, and time are $\sqrt{\hbar/(2m\omega_z)}$, $\hbar\omega_z$, and $1/\omega_z$, respectively.

B. Phase-dependent time evolution

The coupled nonlinear differential equations (20) are numerically integrated using a fourth-order Runge-Kutta method. The initial wave functions $\phi_j(z,0)$ are taken to be the ground-state solutions of

$$\mathcal{L}_z\phi_j(z,0)=\mu\phi_j(z,0)$$

and are normalized as

$$\int |\phi_j(z,0)|^2dz=N_j/N,$$

where N_j is the initial particle number in spin-j. The three $\phi_j(z,0)$ have the same spatial shape.

Solid lines in Fig. 4 illustrate the population in spin-0, obtained using this numerical method, as a function of time for different initial values of relative phase $\theta=2\theta_0-\theta_1-\theta_{-1}$, where θ_j is the phase of the complex wave function $\phi_j(z,0)$, i.e., $\phi_j(z,0)=|\phi_j(z,0)|e^{i\theta_j}$. In this example, the three spin states are initially equally populated. We see that there is a good agreement between the numerical results and the analytical results of Eq. (13), supporting the validity of the SMA in this situation. Solid lines in Fig. 5 and Fig. 6 represent the population averaged over θ and particle number distribution, respectively. Again, good agreement with the SMA results of Sec. II is found.

C. The validity of the SMA

The single-mode assumption assumes that the wave function for each spin component retains the same spatial profile during the time evolution, and the wave function is determined by Eq. (4). The numerical method developed in this section can be used to examine the validity of this assumption. We found the SMA to be well satisfied for small particle number N. This is because the SMA corresponds to neglecting the effect of the nonsymmetric part of the Hamiltonian, H_a, on the evolution of the wave function. For small N, H_a can be safely neglected. However, as N increases, except for certain situations (see below), the contribution from H_a may become non-negligible, and hence the condensate becomes coupled to higher excitation modes, invalidating the SMA.

To study the validity of the SMA in detail, let us examine E_s and E_a, the energy contributed by H_s and H_a, respectively. For the initial wave function defined by Eq. (4),

$$E_a(t=0)=\lambda_a'[L_z^2+2N_0(N-N_0)+2N_0\sqrt{(N-N_0)^2-L_z^2}\cos\theta]. \quad (21)$$

Because the wave function is the ground-state solution of Eq. (4), it minimizes H_s (for fixed total particle number N). In other words, E_s is bounded from below by its initial value. Since the total energy, $E_T=E_s+E_a$, is conserved, it follows that $E_a(t>0)\leqslant E_a(t=0)$. (In practice, the bounding values of E_s, E_a, and the conservation of E_T are used to check the accuracy of our numerical code.) For given N and L_z, E_a of Eq. (21) has a minimum value $(E_a)_{\min}$.

(i) For $\lambda_a'>0$,

$$(E_a)_{\min}=\begin{cases}\lambda_a' L_z^2 & \text{for } L_z\neq 0 \text{ when } N_0=0\\ 0 & \text{for } L_z=0 \text{ when } N_0=0 \text{ or } N, \text{ or } \theta=\pi.\end{cases} \quad (22)$$

(ii) For $\lambda_a'<0$,

$$(E_a)_{\min}=\lambda_a' N^2 \text{ when } N_0=\frac{N}{2}\left(1-\frac{L_z^2}{N^2}\right) \text{ and } \theta=0. \quad (23)$$

Thus we can take the following as the criterion for the validity of the SMA:

$$\Delta E_a=E_a(t=0)-(E_a)_{\min}\ll N\hbar\omega_z \quad (24)$$

because if Eq. (24) is not satisfied, H_a can contribute enough energy to couple the population into higher modes (the excitation energy per atom is roughly $\hbar\omega_z$). For a general initial spin configuration, we notice that ΔE_a increases as $\lambda_a' N^2 \sim N^{5/3}$. Therefore, the SMA breaks down when N is sufficiently large. For the parameters used in our calculations (see Fig. 4 caption) and the initial state with all three spin components are equally populated and $\theta=0$, we estimated from Eq. (24) that in order for the SMA to be valid, N should be much less than $N_{\max}\approx 4\times 10^4$. Our numerical calculations confirm such an estimation by showing that the SMA is satisfactory up to $N\approx 10^4$. Note that $N_{\max}$ scales as $1/\sqrt{\omega_z}$ (assuming η is fixed), hence for a weaker trap, the SMA works for larger N. There are also initial spin configurations such that ΔE_a does not carry the $N^{5/3}$ dependence (for example, the case when most atoms are in the spin-0 state and $\lambda_a'>0$). These configurations correspond to the states which have energies very close to the ground-state energy. In those cases, the internal spin-mixing dynamics essentially do not affect the external spatial wave function even for large particle numbers. In particular, when the initial condition satisfies $\Delta E_a=0$, the system is in a stationary state such that the population in each spin component does not change during the time evolution, i.e., *there is no spin-mixing under such conditions*. A closer examination shows that condition (23) corresponds to the fact that the system is in the eigenstate $|\varphi_+\rangle$ of Eqs. (11) [16].

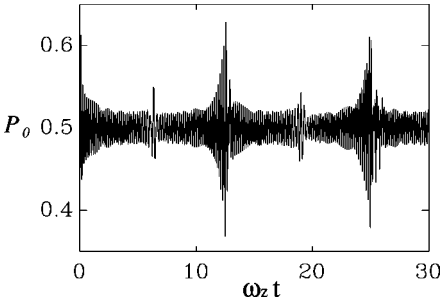

FIG. 7. Population of spin-0 component as a function of time for $\theta=0$ (numerical results). Same parameters as in Fig. 4, except for $N=10^6$.

To illustrate the spin-mixing dynamics when the SMA becomes invalid, we show in Fig. 7 a similar plot as Fig. 4, but with a much larger N. In this case, the complex oscillatory structure obtained from the numerical calculations is quite different from the simple harmonic oscillation predicted by the SMA (not shown). Such behavior indicates the existence of higher excitation modes induced by H_a. The density profiles at different times are illustrated in Fig. 8, where initially all three spin components are equally populated and have the same density profiles. For small N (left column), the density profiles do not vary much in time. In contrast, for large N (middle column), we see that a ''fishbone'' structure develops in the density profiles, and the spa-

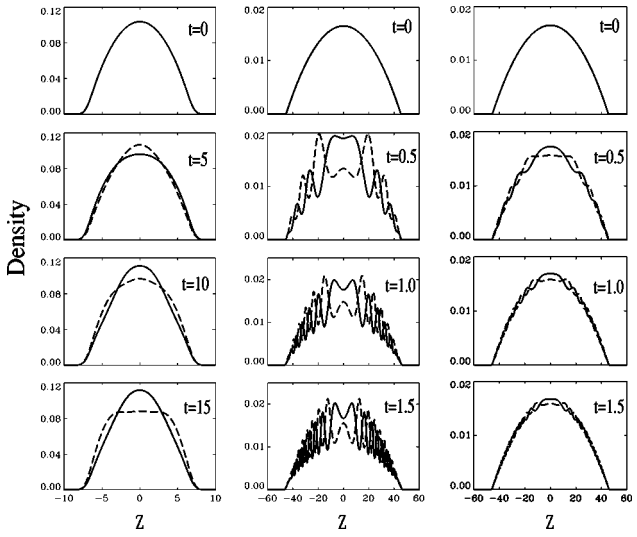

FIG. 8. Variation of the density profiles of the condensate. Solid lines: Density of the spin-(± 1) component; dashed lines: density of spin-0 component. The density is normalized to 1. Initially, $n_1=n_0=n_{-1}=1/3$ and the relative phase $\theta=0$. Left column: $N=4000$, $\theta=0$; middle column: $N=10^6$, $\theta=0$; right column: $N=10^6$, averaged over 200 initial relative phases θ which are uniformly distributed over $(0,2\pi]$.

tial variations for spin-0 and spin-(± 1) components are complementary to each other, i.e., the maxima of the former corresponds to the minima of the latter and vice versa. However, this structure will be smoothed out when the initial phases are randomized. The right column of Fig. 8 shows the density profiles averaged over 200 values of θ uniformly distributed over $(0,2\pi]$. This smoothing effect makes Eq. (16) valid even for large particle numbers. We observe a similar effect if the wave functions are averaged over initial particle numbers which have distributions with finite width as shown in Fig. 6.

The development of complex structures is quite common in systems with nonlinear interactions. For example, when two optical beams are copropagating in Kerr media, cross-phase modulation can lead to a transverse modulation instability, which in turn manifests itself as spatial modulations of the beam profiles — oscillatory patterns appear in the profiles of the two initially smooth Gaussian beams [17]. Figure 8 clearly demonstrates that the spinor condensate is another system that can display such rich behavior. Modulation instability induced by nonlinear interactions has also been studied in the context of two-component condensates [18], where it has been shown that strong repulsive intercomponent interactions intend to break the spatial symmetry of the condensate wave functions.

IV. CONCLUSIONS

In conclusion, we have investigated the spin-mixing dynamics of a spinor condensate with ground-state angular momentum $f=1$ and identified different time scales in the spin-mixing process. To study this, we first used an angular momentum algebraic method under the assumption of a spatially invariant wave function and a Fock state representation of the condensate. Next, we developed a set of semiclassical mean-field equations with the assumption that the condensate is in a coherent state. Finally, we compared the semiclassical results with numerical calculations taking our study beyond the SMA and examined the evolution of the density profiles of the condensate.

From this study, we have found that the evolution of the spinor condensate is sensitive to its initial phase and population distributions. The relative populations of the system will oscillate and exhibit nonlinear behavior due to the mean-field interactions. Similar behavior is also found in nonlinear Josephson-type oscillations of a two-component condensate composed of two spin states of ^{87}Rb [19]. However, the oscillations studied in Ref. [19] are induced by external laser fields, while here, they result from the internal atom-atom interactions. Therefore, the eigenfrequency Ω we found in Eq. (15) can be interpreted as a kind of collective excitation frequency associated with the spin degree of freedom [20].

We have also shown that a steady state can be reached if either the initial phase or population is not well determined but displays fluctuations instead. These steady states are achieved purely as a result of nonlinear spin-mixing interactions instead of dissipation due to the coupling to a thermal reservoir.

We have studied the limit of the validity of the single mode approximation and found that complex structures will appear in the density profiles during the time evolution when the SMA becomes invalid. We attribute this behavior as a result of the modulation instability induced by the nonlinear interactions.

As we have shown in this paper, the dynamics of a spinor condensate is extremely rich. In our treatment, noncondensate atoms have been neglected. These atoms may play an important role at finite temperatures. However, the noncondensate effects may be reduced by lowering the temperature. Our work has not taken the magnetic field into account, the presence of which will certainly affect the properties of the spinor condensate: The longitudinal magnetic field will shift the energy levels of the spin states through the Zeeman effect, while the transverse magnetic field will provide extra coupling between the different spin states. We hope to study these effects in a future publication.

ACKNOWLEDGMENTS

This research was supported by NSF Grant Nos. PHY-9415583 and PHY-9457897, and by the David and Lucile Packard Foundation. We thank Professor G. Shlyapnikov for many useful discussions. C.K.L. acknowledges support from Chinese University of Hong Kong Direct Grant No. 2060148.

[1] C. J. Myatt, E. A. Burt, R. W. Ghrist, E. A. Cornell, and C. E. Wieman, Phys. Rev. Lett. **78**, 586 (1997).
[2] M. R. Matthews, D. S. Hall, D. S. Jin, J. R. Ensher, C. E. Wieman, E. A. Cornell, F. Dalfovo, C. Minniti, and S. Stringari, Phys. Rev. Lett. **81**, 243 (1998).
[3] C. K. Law, H. Pu, N. P. Bigelow, and J. H. Eberly, Phys. Rev. A **58**, 531 (1998).
[4] C. M. Savage, J. Ruostekoski, and D. F. Walls, Phys. Rev. A **57**, 3805 (1998).
[5] D. S. Hall, M. R. Matthews, J. R. Ensher, C. E. Wieman, and E. A. Cornell, Phys. Rev. Lett. **81**, 1539 (1998); D. S. Hall, M. R. Matthews, C. E. Wieman, and E. A. Cornell, *ibid.* **81**, 1543 (1998).
[6] D. M. Stamper-Kurn, M. R. Andrews, A. P. Chikkatur, S. Inouye, H.-J. Miesner, J. Stenger, and W. Ketterle, Phys. Rev. Lett. **80**, 2027 (1998); J. Stenger, S. Inouye, D. M. Stamper-Kurn, H.-J. Miesner, A. P. Chikkatur, and W. Ketterle, Nature (London) **396**, 345 (1998).
[7] Tin-Lun Ho, Phys. Rev. Lett. **81**, 742 (1998).
[8] T. Ohmi and K. Machida, J. Phys. Soc. Jpn. **67**, 1822 (1998).
[9] Elena V. Goldstein and Pierre Meystre, Phys. Rev. A **59**, 1509 (1999).
[10] C. K. Law, H. Pu, and N. P. Bigelow, Phys. Rev. Lett. **81**, 5257 (1998).
[11] Weiping Zhang and D. F. Walls, Phys. Rev. A **57**, 1248 (1998).
[12] Liwei Wang, R. R. Puri, and J. H. Eberly, Phys. Rev. A **46**, 7192 (1992).

[13] Ying Wu, Phys. Rev. A **54**, 4534 (1996).
[14] Because of the discreteness of the energy spectrum, we will see revivals at much longer time scales which are not shown in the figure. Therefore, the ''steady state'' shown in Figs. 1–3 is not really steady. However, we define our steady state to be the state at which the system stays for a time much longer than any other time scale.
[15] K. Huang, *Statistical Mechanics* (Wiley, New York, 1987).
[16] The states satisfying condition (23) are also stationary states for a condensate with $\lambda_a'>0$ since it represents the eigenstate $|\varphi_+\rangle$, even though in this case $\Delta E_a \neq 0$.
[17] G. P. Agrawal, J. Opt. Soc. Am. B **7**, 1072 (1990); W. J. Firth, A. Fitzgerald, and C. Paré, *ibid.* **7**, 1087 (1990).
[18] E. V. Goldstein and P. Meystre, Phys. Rev. A **55**, 2935 (1997); H. Pu and N. P. Bigelow, Phys. Rev. Lett. **79**, 1130 (1998); P. Öhberg and S. Stenholm, Phys. Rev. A **57**, 1272 (1998); D. Gordon and C. M. Savage, *ibid.* **58**, 1440 (1998); B. D. Esry and C. H. Greene, *ibid.* **59**, 1457 (1999).
[19] J. Williams, R. Walser, J. Cooper, E. Cornell, and M. Holland, Phys. Rev. A **59**, R31 (1999).
[20] In the case of a condensate trapped in a double-well potential, coherent oscillations of relative population between the two wells will also occur due to the atom-atom interactions, a phenomenon analogous to the spin-mixing dynamics of the spinor condensate. See, for example, G. J. Milburn, J. Corney, E. Wright, and D. F. Walls, Phys. Rev. A **55**, 4318 (1997); S. Raghavan, A. Smerzi, S. Fantoni, and S. R. Shenoy, *ibid.* **59**, 620 (1999).